Polymer 318 (2025) 127970

Contents lists available at ScienceDirect

Polymer

journal homepage: www.elsevier.com/locate/polymer

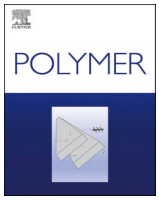

Advanced characterization of recycled polyolefins: A holistic approach to study their microstructure and contaminations

Davide Tranchida [2,*], Dietmar Salaberger [2], Lada Vukusic [2], Gerhard Hubner [2], Mithun Goswami [2], Andreas Albrecht [2], Susana Filipe [1,2]

Borealis Polyolefine GmbH, Innovation Headquarters, St. Peterstr. 25, 4021 Linz, Austria

ARTICLE INFO

Keywords:
Recycling
Polyolefins
Contaminations

ABSTRACT

Achieving the detailed knowledge of recycled materials composition is a formidable task due to the presence of organic and inorganic contaminations. Additionally, the complexity of the microstructure is far superior to the one of virgin materials where the production process is well controlled. Nonetheless, this task is of paramount importance because properties are affected in crucial ways. In this work we studied recycled polyolefin grades with several techniques, in particular through their adaptation to the analysis of this class of materials, to combine the information and obtain a detailed knowledge of their characteristics. Thermogravimetric Analysis (TGA), X-Ray Fluorescence (XRF), X-Ray Computed Tomography (CT) and Scanning Electron Microscopy (SEM) were used to characterize inorganic contaminations. CT and Fourier Transform Infrared Spectroscopy (FTIR) were used to characterize organic contaminations. Microstructure details were evaluated by Nuclear Magnetic Resonance (NMR) and fractionation and thermal analysis methods. Also the limitations of the various techniques are addressed.

1. Introduction

On one hand, in order to meet the challenging ambitions spurred both by regulatory and societal pressure for improving the volume of recycled plastics [1], new and more advanced applications need to be targeted by recycled materials [2]. On the other hand, it is well known that recycled materials are characterized by the presence of both organic and inorganic contaminations as well as degradation, which may complicate their use in more challenging applications. In addition, due to the uncontrolled feedstock, the molecular structure may often be more complex than virgin materials, which are produced under very controlled conditions and with strict targets and quality control analysis.

Automotive applications are good examples for the need of high quality recycled materials, since the very high requirements in this application area sometimes even exclude the use of recycled materials as it is the case for e.g. odour issues [3]. Alternatively, proper care needs to be taken in the selection of the recycled material, as done by Bunjes et al. [4], who focused on the use of pre-consumer recycled materials since the post-consumer recycled ones were considered too contaminated. This aspect indeed highlights the importance of a proper characterization. The attempts to use recycled materials into advanced applications also encompass additive manufacturing [5,6], nanocomposites [7], structural applications [8,9], glass fibres filled composites [10].

The need for extending the sources of recycled materials is witnessed by studies investigating e.g. electrical and electronic waste [11,12], packaging [13,14], printers [15], agricultural sectors [16,17]. The variety of the possible feedstock is obviously linked to the variety of contaminations and molecular structures that can be found in recycled materials, and this is clearly linked to the challenges for their proper characterization and thus to the possibilities to use them in advanced applications.

Several works in the literature investigated the final properties of various recyclate composition, either in neat state or in blend with virgin materials and in particular concerning mechanical [18,19] or electrical properties [20].

Concerning the study of composition, typically the analysis was

* Corresponding author.
E-mail address: davide.tranchida@borealisgroup.com (D. Tranchida).
[1] Currently at: Global Change and Sustainability Institute, Institute for Advanced Studies and Research, University of Évora, Pólo da Mitra, Ap. 94, 7006-554 Évora, Portugal.
[2] Dedicated to Jens Reussner on the occasion of his retirement.

https://doi.org/10.1016/j.polymer.2024.127970
Received 12 September 2024; Received in revised form 25 November 2024; Accepted 19 December 2024
Available online 20 December 2024

performed with a few techniques. Due to their simplicity, Differential Scanning Calorimetry (DSC), thermogravimetric analysis (TGA) and Fourier-Transform infrared (FTIR) spectroscopy were often used to gain a general picture of respectively inorganic and organic contaminations as well as the main polymeric composition [21–23]. Gall et al. [21], beyond highlighting the effect of contaminations on impact strength, identified the presence of calcium carbonate from the TGA analysis, also raising the point that this would artificially increase the density measurements of PE-based recyclates. Since density is a very commonly used engineering parameter to define a PE, this finding highlights the need for detailed characterization to properly develop recyclate materials. Cozzarini et al. [22] coupled the information from FTIR and DSC measurements, noting that the quantification of the components was not possible through DSC alone. They however noted how the information about the presence of LDPE cannot be obtained by FTIR, while some qualitative information could be derived from DSC. Stoian et al. [23] combined the information from DSC, TGA, and FTIR to study the optimal proportion of virgin and recycled materials to be used to achieve the best mechanical properties, thus highlighting the role of a precise characterization to best design the recipe of compounds.

In rare cases, more advanced fractionation techniques like Temperature Rising Elution Fractionation (TREF) were used to investigate the details of composition, for PE [24,25] based recyclates or model blends. However the use of model blends, although necessary for the understanding of the results from the technique, limits the deep understanding of the challenges posed by real recycled materials with a very complex composition. Also in the case that recyclates were used, to the best of our knowledge no insight was given on the difficult cases where coelution of fractions from different materials is obtained. Scanning Electron Microscopy (SEM) [26,27] and AFM-IR [28] were also used to study the morphology. AFM-IR in particular provides the chemical information, thus being able to clearly identify PE and iPP fractions as well as organic contaminations with high resolution, although it cannot give information on the inorganic contaminations.

Incidentally the study of recyclates actually pose phenomenal challenges and a few contributions in the literature have investigate adaptations to mechanical [29], fractionation [30], and thermal analysis as DSC [31], isothermal crystallization [32] and Successive Self-nucleation and Annealing (SSA) [33–35].

In this work, we show a very detailed use of the aforementioned techniques together with the use of other standard, e.g. X-Ray Fluorescence (XRF), and new approaches, e.g. in Nuclear Magnetic Resonance (NMR), X-Ray Computed Tomography (CT) to gain a complete picture of the recyclate composition, tackling several small details that may have considerable effects for final properties. We are not able to discuss issues like the effect of geographical origin of the waste stream used in recyclates, and likely this remains the core knowledge of recyclers. However three different lots of the nominally same grade were used, and thus their analysis can shed some light on the effect of seasonal variation of post-consumer recyclates and the variations to be expected from lot to lot.

2. Experimental

Materials. Post consumer recyclate grades were kindly provided by Borealis and used as received. REC1, REC2, REC3 were three different lots, produced not consecutively, of the same commercially available grade. This material is a PE/iPP blend obtained by recycled post-consumer waste from pre-sorted household feedstock. REC4 is a different post-consumer recyclate.

TGA. Thermogravimetric Analysis (TGA) experiments were performed with a TA Instruments TGA 5500. Approximately 10–20 mg of materials were placed in a platinum pan. The temperature was equilibrated at 50 °C for 10 min, and afterwards raised to 900 °C under nitrogen at 20 °C/min in high resolution mode. In this case, the instrument lowers the heating rate with a feedback system if sensing that considerable weight loss is taking place. This ensures that large transitions are not smeared over large temperature ranges due to the continuously increasing temperature. Afterwards the temperature was lowered to 300 °C at 20 °C/min, gas switched to oxygen, and the temperature was raised again to 900 °C. The weight loss in this final step was assigned to carbon black. Two measurements were performed on each material.

XRF. The instrument used for the XRF measurements was a Bruker S4 Pioneer. The instrument was calibrated with proprietary polyolefin based standard sets. The analyses are done under vacuum on a plaque with a diameter of 40 mm and a thickness of 2 mm. Two measurements were performed on each plaque.

CT. The scans were done on a ThermoFisher Heliscan device with a resolution of 10 μm Voxel edge length operated with helical trajectory. 60 kV acceleration voltage with pre-filtering was used to increase contrast between different polymeric materials. Image analysis was performed with Avizo.

Together with 100 pellets for each material, a stack of discs made of different polymers was scanned at once. The average grey values of these reference discs were used to define thresholds for segmenting organic and inorganic inclusions. Pellets and reference materials were placed in a cylindrical sample holder without further preparation.

SEM. Scanning electron microscopy images were taken with a Quanta 200F scanning electron microscope, equipped with an energy dispersive x-ray spectrometer (EDS). Both secondary electron detector and back-scattered electron detector were used, with typical acceleration voltages in the range of 5kV–20kV. Prior to the SEM analysis the specimens were cryo-cut with an ultra cryo-microtome Leica EM UC7 at −100 °C in order to obtain a smooth surface and sputter coated with an Au/Pd alloy (Polaron sputter coater).

For permanganic etching a 1 % w/v solution of $KMnO_4$ in 86%H_2SO_4 acid was used and the specimens were etched for 15 min. After chemical etching the specimens were rinsed with distilled water for approximately 10 min and subsequently placed in H_2O_2 (30 %) for 10 min and stirred. The specimens were rinsed first with distilled water, then with acetone and finally dried.

The RuO_4 used for staining was produced in situ by mixing 40 mg of $RuCl_3$ with 6 ml of aqueous solution of $NaIO_4$ in a 10 ml glass vial. Staining was performed for 20 h at RT in the vapor phase above the reaction liquor. After that the samples were rinsed with water and subsequently with acetone. Finally, approximately 2 μm of overstained surface was removed with microtome at room temperature. Specimens which were stained were not additionally sputter coated.

FTIR. Standard transmission FTIR spectroscopy measurements were performed in Bruker Vertex 70 FTIR spectrometer. The typical spectral window used for the measurements was 4000-400 cm^{-1} with spectral resolution of 2 cm^{-1}. Circa 3 g of the sample to be analysed were molten at 190 °C and pressed in a hydraulic heating press with a 100 μm thick frame. Next, the samples were cooled down in a cold press under the same pressure, in order to control the morphology of the sample. The thickness of each plate was measured before any FTIR measurements. Nine measurements were performed in total, three on each of the three plaques prepared from each materials.

NMR. Quantitative $^{13}C\{1H\}$ NMR spectra were recorded in the solution-state using a Bruker AVNEO 400 MHz NMR spectrometer operating at 400.15 and 100.62 MHz for 1H and 13C respectively. All spectra were recorded using a ^{13}C optimized 10 mm extended temperature probehead at 125 °C. Approximately 200 mg of material was dissolved in approximately 3 ml of 1,2-tetrachloroethane-d2 (TCE-d2) along with approximately 3 mg BHT (2,6-di-*tert*-butyl-4-methylphenol CAS 128-37-0) and chromium–(III)–acetylacetonate (Cr(acac)3) resulting in a 60 mM solution of relaxation agent in solvent [36]. To ensure a homogenous solution, after initial sample preparation in a heat block, the NMR tube was further heated in a rotatory oven for at least 1 h. Upon insertion into the magnet the tube was spun at 10 Hz. Standard single-pulse excitation was employed without NOE, using an optimized tip angle, 1 s recycle delay and a bi-level WALTZ16 decoupling scheme

[37,38]. A total of 6144 transients were acquired per spectra. Quantitative 13C{1H} NMR spectra were processed, integrated and relevant quantitative properties determined from the integrals. All chemical shifts were indirectly referenced to the central methylene group of the ethylene block (EEE) at 30.00 ppm using the chemical shift of the solvent.

DSC. A TA Instruments Q2000 Differential Scanning Calorimeter was used as calibrated with Indium, Zinc, and Tin and operating under 50 mL/min of nitrogen flow. Tzero pans from TA Instruments were used. The employed thermal program consisted of a first heating step to 225 °C to erase the previous thermal history and a cooling step at 10 °C/min. The melting behaviour was obtained by performing a second heating scan to 225 °C at 10 °C/min. For the temperature modulated experiments, the final heating was conducted at 2 °C/min and modulating the temperature with an amplitude of 0.32 °C every 60 s.

A-TREF. A CRYSTAF-TREF model 200 (PolymerChar, Valencia, Spain) was used for performing analytical temperature elution fractionation (a-TREF) analysis. Around 90 mg of the samples was dissolved in 40 ml of TCB stabilized with 250 mg/L 2,6-Di tert butyl-4-methyl-phenol at 160 °C for 150 min. An aliquot of the sample solution was injected into the TREF column. The column oven was stabilized at 110 °C for 30 min and later slowly cooled to 35 °C using a constant cooling rate of 0.1 °C/min. The polymer was subsequently eluted from the column with 1,2,4-trichlorobenzene (stabilized with 250 mg/L 2,6-Di tert butyl-4-methyl-phenol) at a flow rate of 0.5 mL/min at 35 °C for a period of 10 min followed by a temperature increase from 35 °C to 135 °C at a constant heating rate of 0.5 °C/min and a flow rate of 0.5 ml/min. The concentration of the polymer during elution was recorded by an infrared detector. The detector response was plotted as a function of the temperature.

CFC. A CFC instrument from PolymerChar was used to perform the cross-fractionation (TREF x SEC) [39]. A four band IR5 infrared detector was used to monitor the concentration. Roughly 8 mg of the polymer sample was dissolved in 8 ml TCB stabilized with 250 mg/L 2,6-Di tert butyl-4-methyl-phenol for 150 min at 160 °C. Once the sample was completely dissolved an aliquot was loaded into the TREF column and stabilized at 95 °C. The analytical parameters used for analysing the sample are reported in the Supporting Information.

In the second dimension (GPC) 3 PL Olexis columns 1x Olexis Guard columns from Agilent were used as stationary phase. 1,2,4-trichlorobenzene (TCB, stabilized with 250 mg/L 2,6-Di tert butyl-4-methyl-phenol) at 150 °C and a constant flow rate of 1 mL/min was used as eluent. The column set was calibrated using universal calibration with at least 15 narrow molecular weight distribution polystyrene (PS) standards in the range of 0.5 kg/mol to 11 500 kg/mol.

LAOS. The non-linear viscoelastic response was analysed applying Large Amplitude Oscillatory Shear (LAOS). Time sweep measurements were performed on an RPA 2000 rheometer from Alpha Technologies coupled with a standard biconical die. During the course of the measurement the test chamber is sealed and a pressure of about 6 MPa is applied. The LAOS test is done applying a temperature of 190 °C., an angular frequency of 0.628 rad/s and a strain amplitude of 10. In order to ensure that steady state conditions are reached, the non-linear response is only determined after at least 20 cycles per measurement are completed. The Large Amplitude Oscillatory Shear Non-Linear Factor (LAOS-NLF) is defined by:

$$LAOS - NLF = \frac{G_1'}{G_3'} \quad (1)$$

where G_1' is the first order Fourier Coefficient and G_3' is the third order Fourier Coefficient.

Table 1
Content of inorganic contaminations according to XRF and TGA analysis.

	REC1	REC2	REC3	REC4
Carbon black, wt%	0.15 ± 0.07	0.17 ± 0.03	0.05 ± 0.04	–
Chalk, wt%	0.7 ± 0.1	1.0 ± 0.1	1.0 ± 0.1	0.7 ± 0.1
Other ash, wt%	1.4 ± 0.3	1.7 ± 0.2	1.6 ± 0.1	1.5 ± 0.1
Al, ppm	202 ± 4	235 ± 5	249 ± 4	169 ± 2
Br, ppm	31 ± 1	45 ± 3	27 ± 1	13 ± 1
Ca, ppm	2195 ± 21	2616 ± 23	2887 ± 59	1939 ± 1
Cl, ppm	321 ± 23	484 ± 8	493 ± 2	148 ± 11
Cu, ppm	40 ± 2	39 ± 3	43 ± 4	n.a.
Fe, ppm	216 ± 1	235 ± 6	220 ± 11	61 ± 6
Mg, ppm	214 ± 5	185 ± 1	221 ± 13	593 ± 5
Na, ppm	105 ± 7	166 ± 4	162 ± 21	78 ± 1
P, ppm	72 ± 3	75 ± 1	83 ± 1	45 ± 1
S, ppm	159 ± 15	198 ± 6	217 ± 1	35 ± 1
Si, ppm	719 ± 21	778 ± 4	878 ± 11	795 ± 4
Ti, ppm	3759 ± 33	3964 ± 33	4059 ± 71	6480 ± 45
Zn, ppm	58 ± 4	75 ± 3	70 ± 1	47 ± 1

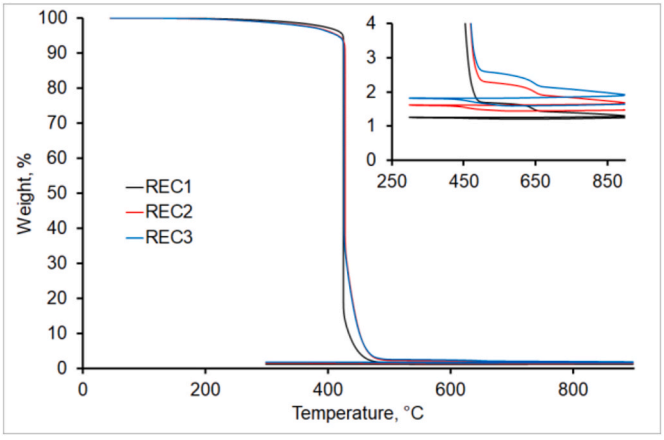

Fig. 1. TGA thermograms for materials REC1-3. The inset shows a zoom on the high temperature range of the measurement, where the weight losses due to the presence of talc and carbon black can be observed.

3. Results and discussion

3.1. Analysis of inorganic contaminations

Due to the simplicity of the analysis together with its high accuracy, TGA analysis is the first choice in order to estimate the content of inorganic contaminations. The thermal history described in the experimental part allows one to evaluate the carbon black content of the material tested. In addition, typically a weight loss at ca. 650 °C is observed, and this can be linked to the loss of CO_2 from $CaCO_3$ [21], which is a filler often present in polyolefin commercial grades. This weight loss is thus stoichiometrically converted into chalk content. The weight measured under N_2 at ca. 850 °C is in general assigned to "ash content" [40], and recycled materials pose particular difficulties to understand its composition since the nature of contaminations cannot be assumed, unlike for virgin grades where the compound recipe used typically guide the assessment of the nature of this ash content without the need of additional analysis.

The results in Table 1 show that overall, all these materials have quite similar content and nature of inorganic contaminations. Fig. 1 in particular compares the full thermograms of the materials REC1-REC3, to highlight the subtle changes lot by lot. The large weight loss attributed to the polyolefin fraction of the materials studied, centred at ca. 430 °C, is similar for the three materials. Additionally, the inset shows the weight loss related to carbon black after lowering the temperature and switching the atmosphere to oxygen. The very low contents of ~0.1

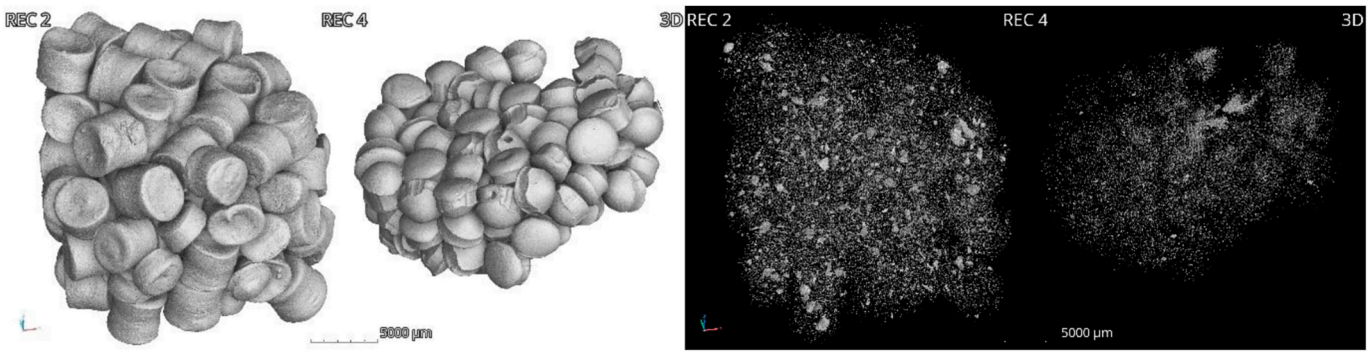

Fig. 2. 3D renderings of pellet surfaces (left); 3D renderings of inclusions with higher density than the surrounding polymeric matrix only (right) both for REC2 and REC4.

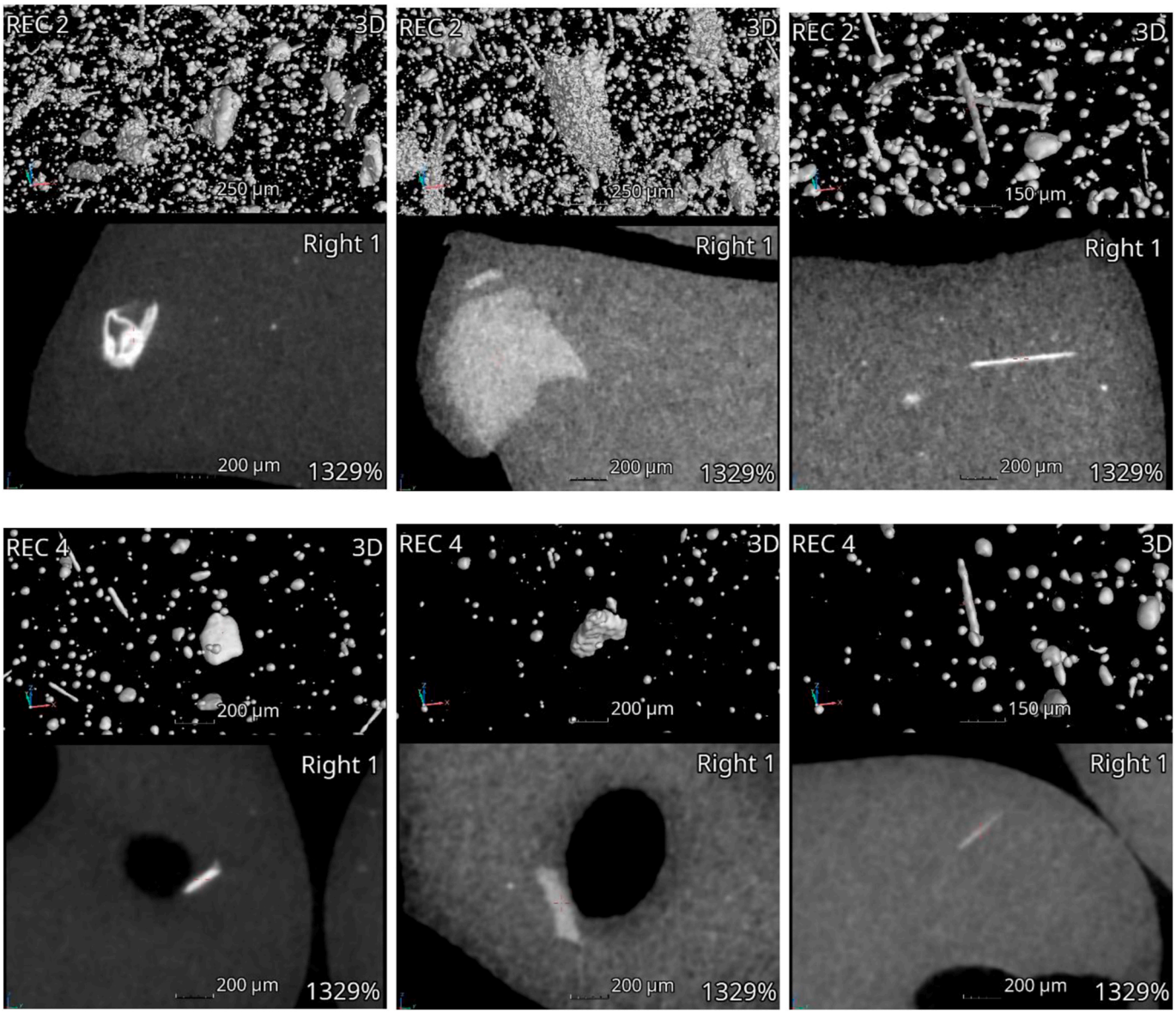

Fig. 3. 3D and cross sectional images of typical contaminants. Inorganic (left), polymeric (middle), glass fibre (right) for REC2 (top row) and REC4 (bottom row).

wt% are clearly well resolved, and albeit being very low content, the knowledge of these values is relevant since already sufficient to impart a grey colour to the material.

The results from the XRF analysis of the four materials used in this study are shown in Table 1, providing additional detail compared to the overall ash content obtained from TGA. One interesting finding is the quantification of Ti, which can be connected to the presence of TiO_2, widely used as a pigment. TiO_2 is known to us to damage glass fibres,

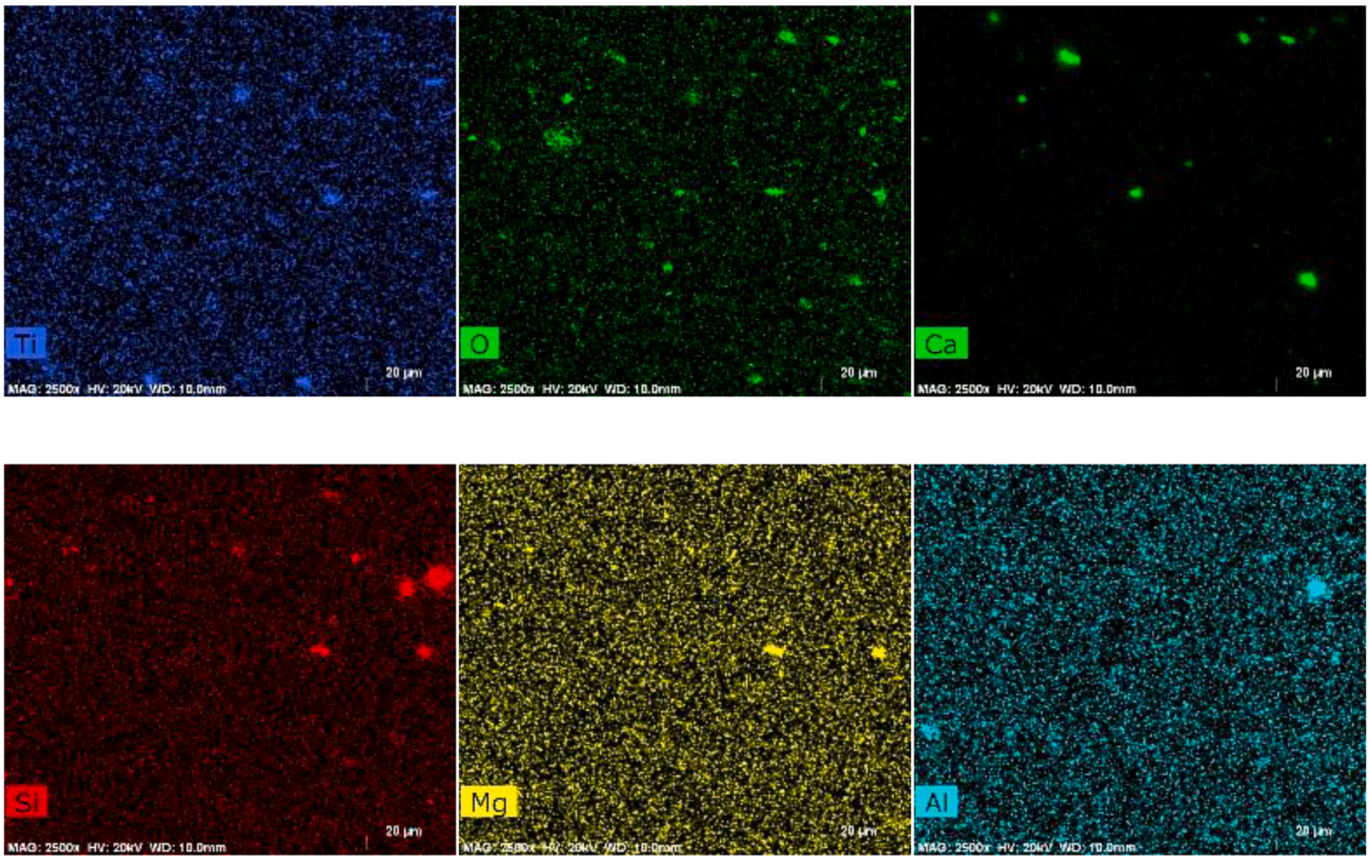

Fig. 4. Elemental distribution from SEM-EDS in REC2 at 2500x magnification, for selected elements. See text for discussion.

and therefore this analysis can provide some hint about the possibility to use these recyclates in new compounds containing glass fibres. Also interesting is the presence of Mg and Si, which are contained in talc that is also a commonly used additive [41]. This analysis can therefore provide information on the amount of talc in the total ash measured by TGA, but also one can notice that the ratio of Mg and Si does not correspond to the expected stoichiometric ratio, with excess Si thus likely linked to the presence of glass fibres especially in REC1, REC2, REC3.

CT analysis with threshold above the grey level relative to the other possibly present polymers with the highest density (e.g. PET) can be used to determine the content of inorganic contaminations, albeit as volume content. Details on the selection of the abovementioned threshold are given in the following. 100 pellets were scanned to generate the images reported in Figs. 2 and 3 for REC2 and REC4 respectively, which leads to data with very good statistical power. The achievable resolution of 10 µm Voxel edge length defines the minimum detectable size of contaminants to ca. 23 µm. Therefore inorganic contaminations can be easily determined by CT, and in particular 3D data is generated that allows to quantify contamination content and to analyse the 3D shape of individual particles. Fig. 2 shows the outer surface of the pellets as well as all contaminants with higher density.

The shape of the inorganic contaminants can be quite complex, forming foil like structures or can be rather spherical [42]. Some glass fibres are also present, as it can be identified by shape and grey value (Fig. 3) [43].

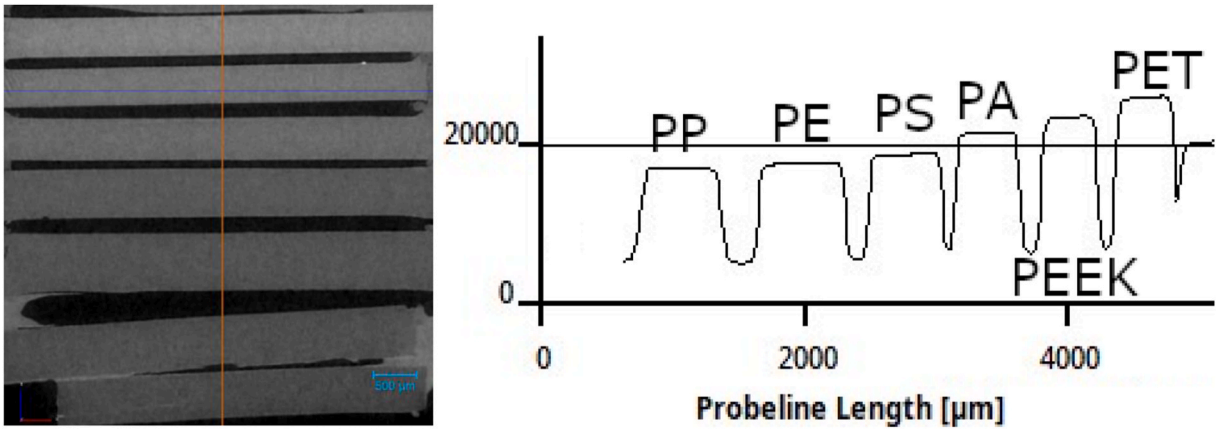

Fig. 5. Cross sectional image of polymer reference stack with grey value distribution along vertical axis. Note that PE and iPP are in this case neat materials, without fillers.

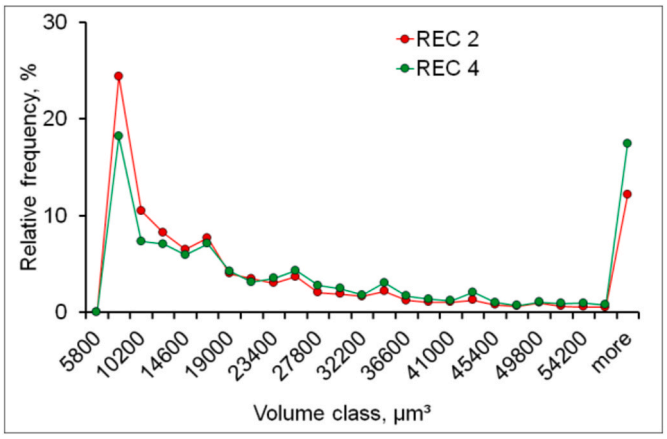

Fig. 6. Size distribution of all segmented inorganic contaminants in absolute volume classes.

Additional information about the size and shape of the contaminants and specifically their spatial distribution is provided by SEM analysis, and in particular by elemental mapping. An example of such mapping for REC2 is shown in Fig. 4, while elemental maps for the other materials are reported in the Supporting Information. Combining the information from the shape of the particles and the overlapping elements in elemental maps one can draw conclusions about their origin: small, spherical particles where the enriched signal from Ti overlaps with the one from O can be inferred to be related to the presence of TiO_2, while irregularly shaped particles containing Ca and O are related to chalk, platelet-like particles with Mg, Si, O and sometimes Al are talc particles, and finally particles containing Si and O are mostly likely glass. This analysis then somewhat combines the elemental info from XRF with the imaging of particles from CT, however with the usual drawback for any microscopy technique that the area imaged is relatively small and thus with less statistical relevance than the information from the two other techniques mentioned above.

3.2. Analysis of polymeric contaminations

It is also possible to identify polymeric contaminants with higher density than the expected polyolefins from CT data by applying different thresholds. The proper threshold to use for each material can be determined by using the grey values obtained from a reference stack (Fig. 5), made of the most commonly found contaminations. Considering PET as the polymer with the highest density reasonably present in recyclates, one can use this grey level in particular to fix the highest threshold used to evaluate the content of inorganics. Thresholds set step by step in lower intervals allow one to, in principle, identify particles made of the various polymers. This approach has the potentialities to work very well, as shown in the Supporting Information where the quantification of the content of several different polymeric contaminations was possible on different materials than the ones used in this study.

A possible issue however is given by the presence of heavy elements like Ti or Ca, present e.g. in titania or chalk particles with very fine distribution and in particular in the form of particles with size smaller than the size that can be resolved properly. These artificially increase the average threshold of the matrix, and if the content of these elements is very high, then the average value of the polyolefin matrix becomes comparable to the grey level found for the neat PS and PA in the calibration stack. Therefore it would not be possible to detect polymeric particles with relatively low density like PS and PA, since the grey level related to the density of these materials matches the increased grey level of the polyolefin matrix with finely dispersed particles. Two examples of polymeric contaminants with high density are shown in Fig. 3, middle. Grey value indicates that these are PET particles.

Table 2
Additional details on the contaminants by CT and FTIR.

Technique	Material	REC1	REC2	REC3	REC4
CT	inorganic, vol%	n.a.	0.11	n.a.	0.01
	polymeric, vol%	n.a.	0.21	n.a.	0.02
	total, vol%	n.a.	0.32	n.a.	0.03
FTIR	PA, wt%	0.4 ± 0.1	0.6 ± 0.1	0.6 ± 0.1	n.a.
	PS, wt%	1.7 ± 0.5	2.4 ± 0.7	2.4 ± 0.6	n.a.

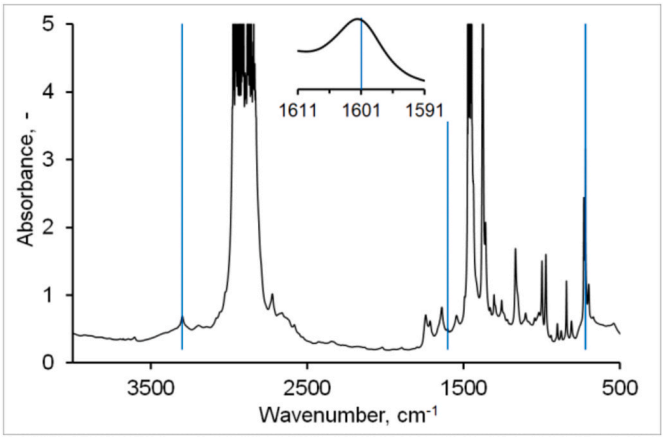

Fig. 7. FTIR spectrum of REC3. Specific bands used for quantification of PE, PS and PA are highlighted.

Additionally, the CT analysis provided a crucial information. Fig. 6 shows the size distribution of particles segmented by using a grey level larger than the one measured in the calibration stack for PET. This is therefore the size distribution of segmented inorganic particles. The total vol% of these particles was lower than what measured for inorganic contaminations by TGA, see Tables 1 and 2, since the well dispersed and small particles, e.g. talc sheets and titania particles, were not visible in the CT data. However this analysis provided information on the amount and size distribution of agglomerates of the inorganic particles, i.e. forming not well dispersed clusters, which could be responsible for example for mechanical failures. Therefore, although strictly speaking less accurate than TGA in characterizing the actual content of inorganic contaminations, CT analysis could still provide very focused information on the part of the contaminations that could have detrimental effects on properties.

To overcome the issue with these materials of not being able to clearly segment PS and PA particles, FTIR spectroscopy was performed. Indeed, many different organic contaminants can be included in the quantification, provided at least one characteristic bands of the contaminants are observable separately and not strongly overlapped with others [44]. Hence, in principle, it is possible to include quantifications also of e.g. EVA, PVC, Acrylonitrile etc in addition to the components reported in Table 2. The first step of accurate quantitation from FTIR spectra is thus the selection of suitable vibration bands, based on their linear increase in intensity with the amount of the component concentration and due to their expected isolation from the rest of the bands in a typical polyolefin matrix.

For the analysis of PA and PS, respectively the NH stretching vibration band at 3300 cm^{-1} and the styrene ring vibration at 1601 cm^{-1} were used. The intensity of these bands was evaluated, normalized by the known sample thickness, and used in correlations developed from model systems with known amount of these polymers. The content of other polymers, e.g. PET and PVC, could also be evaluated with this approach based respectively on the aromatic ring vibration at 1410 cm^{-1} and the C–Cl stretching vibration at 616 cm^{-1}. Fig. 7 shows one

Table 3
Content of iPP, PE, LDPE as measured by various techniques.

Technique	Fraction	REC1	REC2	REC3	REC4
FTIR	iPP, wt%	76	58	54	n.a.
	PE, wt%	19	38	42	n.a.
NMR	iPP, wt%	66	51	50	91
	PE, wt%	31	47	48	7
	LDPE, wt%	n.m.	18	14	n.m.
DSC	iPP, wt%	69	54	54	92
	PE, wt%	28	44	44	6
	LDPE, wt%	8	24	21	0
CFC	iPP, wt%	71	43	47	79
	PE, wt%	21	51	47	9

n.a. Not available.
n.m. Not measurable.

spectrum for REC3, highlighting in particular the bands used for the quantifications reported in Table 2. Since these polymers are immiscible with polyolefins, it is reasonable to expect, as it is shown below, that they are present in the form of particles, which could for example trigger mechanical failures by being fracture initiation points. Most notably in the spectrum is the high intensity of the band at 3300 cm^{-1}, indeed related to relatively high PS content. Other spectra are reported in the Supporting Information. Additionally, the presence of inorganic components such as talc and chalk can be inspected using the bands at ca. 670 cm^{-1} and 875 cm^{-1} respectively. Further, the observation of the broad hump between ~490 cm^{-1} to ~790 cm^{-1} indicates the presence of TiO_2.

3.3. Analysis of polyolefin composition

Additionally, the CH_2 rocking band at 721 cm^{-1} was used to quantify the PE content in the materials. In particular, the area under this band was evaluated and, after normalization by sample thickness, used in a correlation developed from model materials. The results are reported in Table 3 and compared to the other techniques discussed in the following.

The basic ^{13}C NMR spectra stack plot between REC1-4 (Fig. 8) in the aliphatic region between 10 ppm and 50 ppm shows presence of main signals from both iPP (Sαα, Tββ and Pββ) [45,46] and PE(Sδδ) [47,48] in different ratios. REC4 shows only low amounts of PE compared to REC1-3 comprising significant amounts of PE. The zoomed in spectra stack plot in Fig. 8 shows detailed fingerprint of microstructural elements by signals resonating at different chemical shifts [49,50]. When qualitatively inspecting the observed signals we find good agreement between the spectra of REC1-3 and we find the microstructure of REC4 to be different.

Quantitative ^{13}C NMR spectra were processed, integrated and the relevant quantitative properties determined from the integrals according to the procedure described in another contribution from our group [51], especially developed for the analysis of polyolefin recyclates. Results for the PE and iPP content are reported in Table 3. The content of LDPE can be estimated assuming the B5 branch, which only arises from ethylene being polymerised under high pressure process and that is not observable in low pressure polyethylene [52–55], being almost constant in LDPE.

The DSC traces, for the heating flow during the second heating run and for the non-reversing heat flow during a further heating run, are

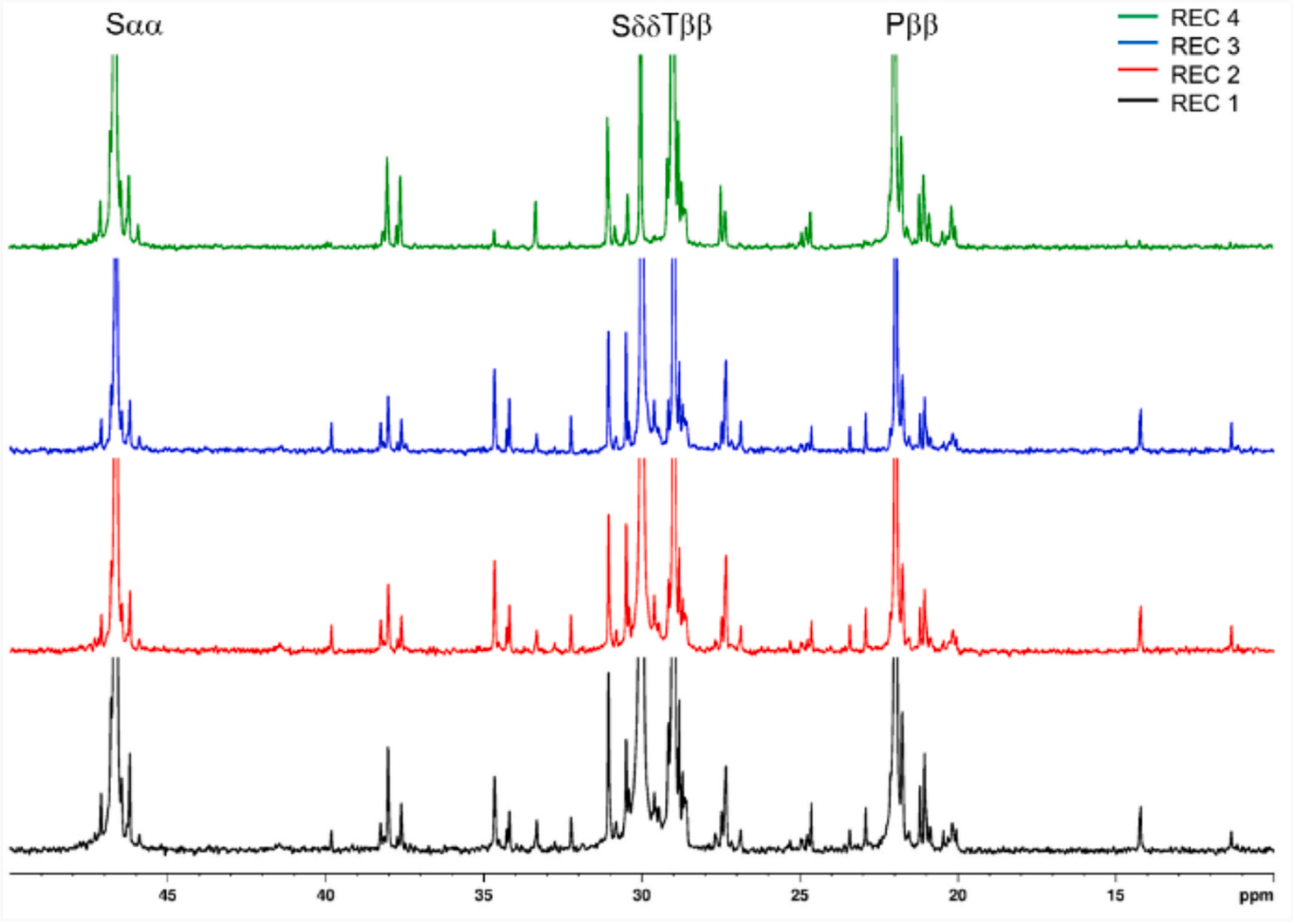

Fig. 8. ^{13}C NMR spectra stack plot REC1 – REC4, zoom in 10 ppm–50 ppm.

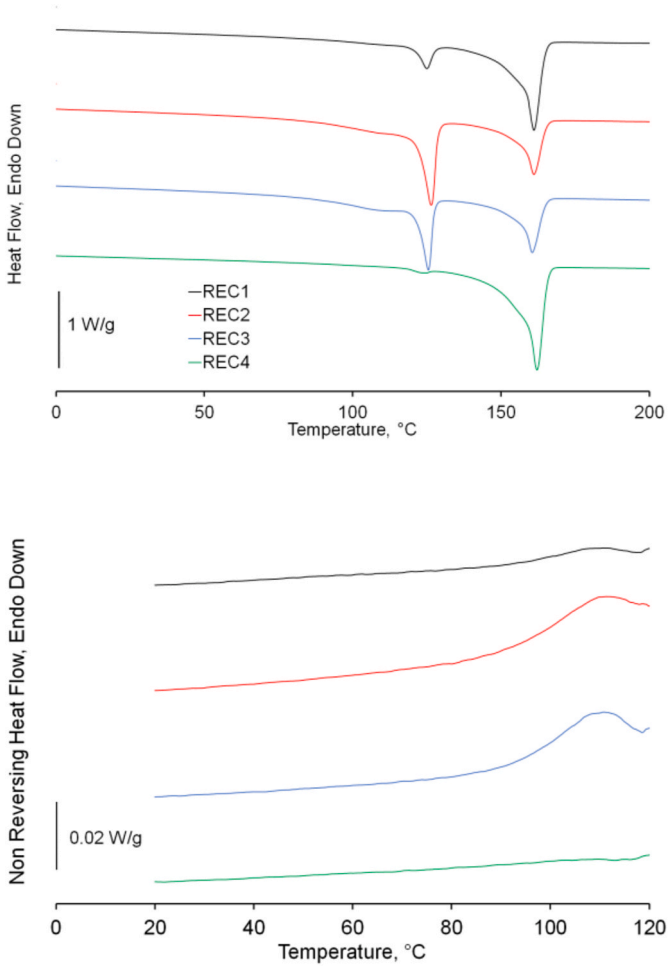

Fig. 9. Results of DSC and temperature modulated DSC from all the materials studied in this work.

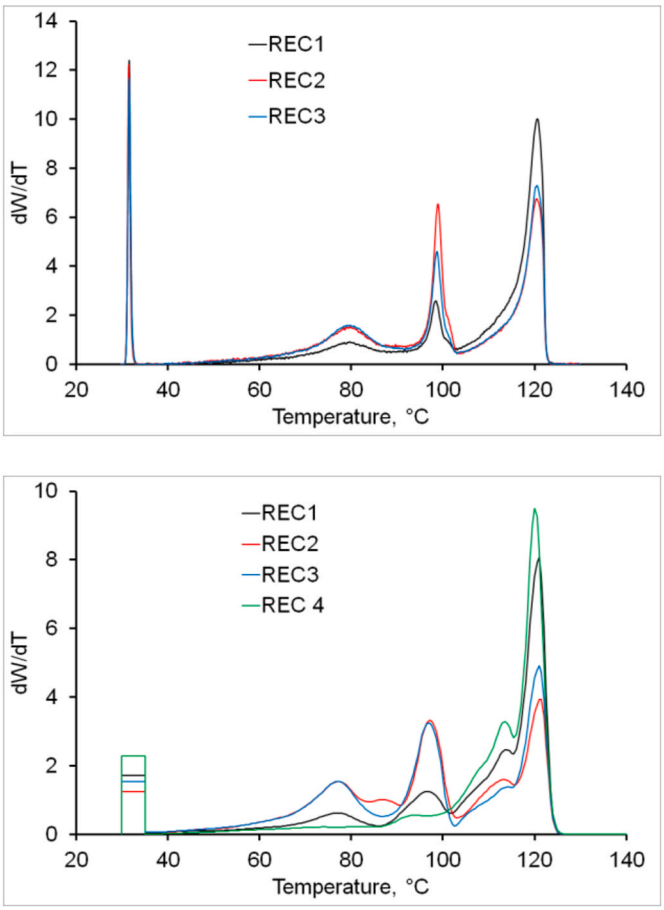

Fig. 10. TREF profile obtained by analytical-TREF (top) and from CFC (bottom).

shown in Fig. 9. The very different size of the PE melting peak, centred at ca. 127 °C clearly hints to the very different PE content of these materials. In particular, REC2 and REC3 show a very high content of PE, while this was very small in the case of REC4. DSC analysis is, to the best of our knowledge, also the only technique that can provide an indication of the PE fraction density, according to its correlation to the melting peak temperature [27]. The LDPE content of the PE fraction can be investigated from the non-reversing heat flow, and the traces in Fig. 9 show the same qualitative information as for the overall PE content, i.e. REC2 and REC3 are not only richer in PE, but also in LDPE compared to the materials REC1 and REC4. The values obtained according to ref. 27 are reported in Table 3 and further compared to the other techniques used in this study.

TREF and CFC were performed to evaluate especially the PE fraction and the iPP fraction in a more detailed analysis.

The TREF profiles obtained from a-TREF and CFC for REC1-4 are shown in Fig. 10. As expected smoother TREF profile are obtained from a-TREF, which applies a continuous elution process, compared to the one obtained from CFC analysis, shown in the following, where a stepwise elution process is selected to enable the characterisation of the molecular weight distribution (MWD) of the individual fractions.

Considering the iPP fraction as the one eluting between 103 and 130 °C with a peak maximum at around 120 °C, the TREF profiles confirm the findings from DSC and NMR analysis with a higher amount of iPP content for REC4, followed by REC1 and then REC 3 and 2. Besides the iPP fraction, the HDPE fraction of the overall PE phase is clearly distinguished by a sharp peak centred at ~98 °C in the elution

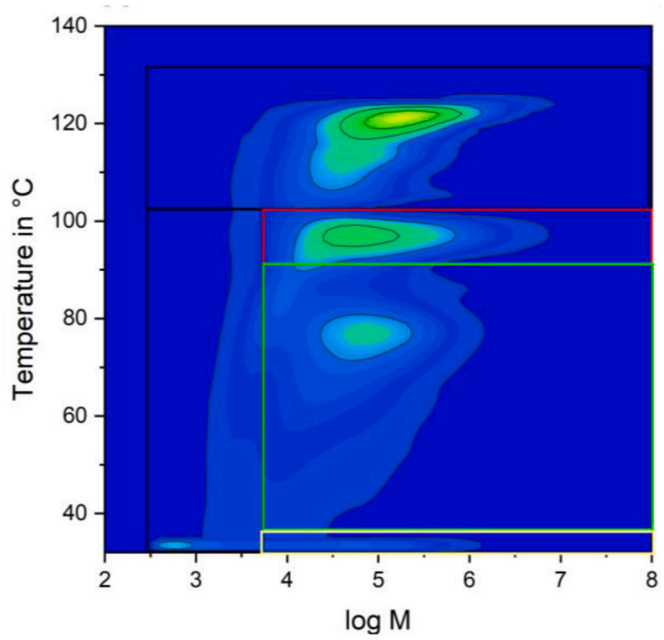

Fig. 11. Example of CFC contour plot of REC3. The area highlighted corresponds to assigned elution area in CFC for iPP (black), the coelution area of HDPE and ethylene-propylene copolymer (red), coelution of LLDPE and LDPE (green) and the elastomer region corresponding to EPR rubber and other elastomers (yellow). (For interpretation of the references to colour in this figure legend, the reader is referred to the Web version of this article.)

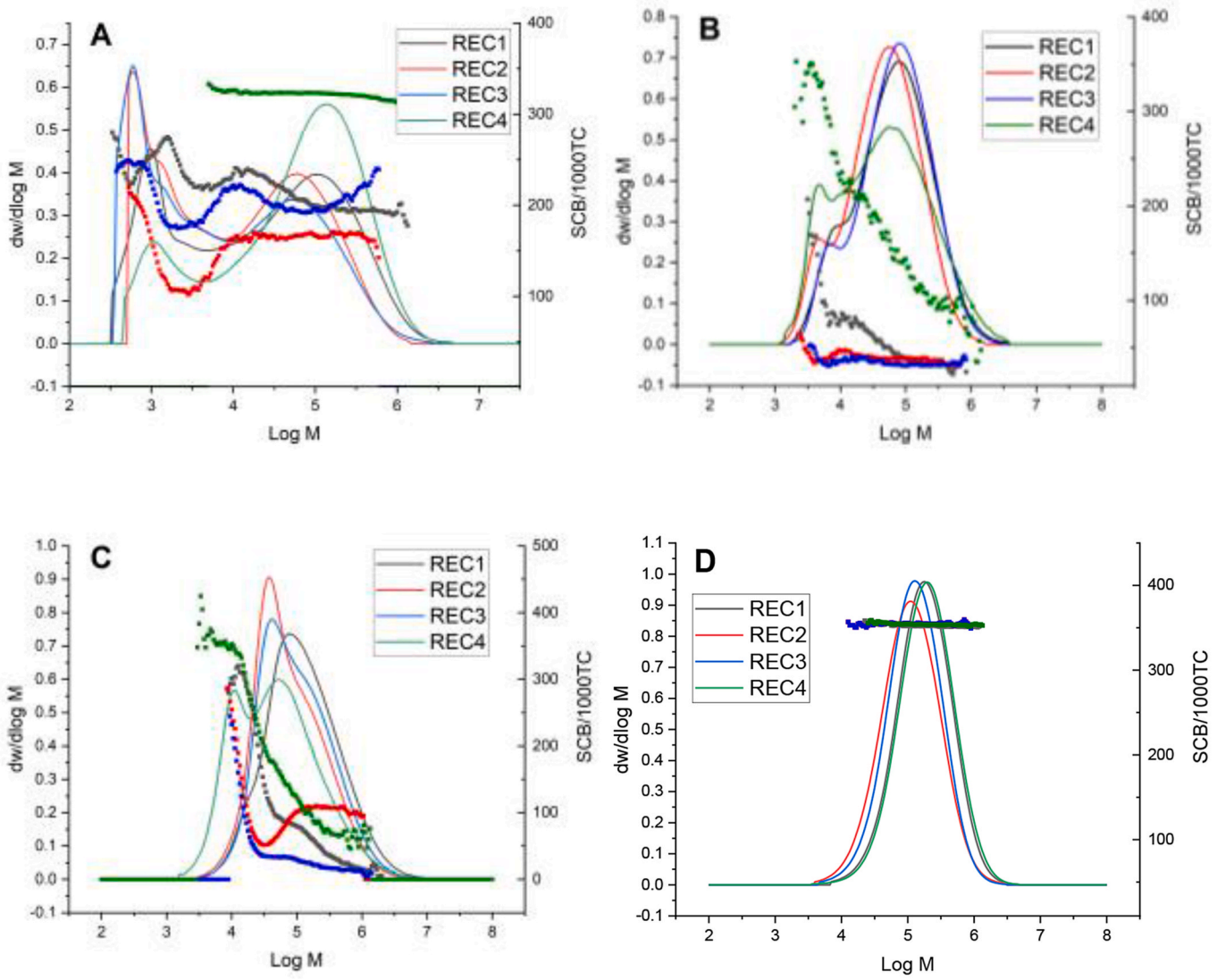

Fig. 12. GPC-IR of CFC fractions eluting at 35 °C (A), 75 °C (B), 95 °C (C) and 121 °C (D).

region between 90 and 103 °C. However, since these are recycled materials with uncontrolled microstructure, it has to be noted that also the polypropylene copolymer (ethylene/propylene copolymer) elutes in the same TREF region. Between 35 and 90 °C, the LDPE/LLDPE elution region is clearly resolved [56]. Below 35 °C, the fraction soluble in the used solvent elutes. This fraction is composed of low molecular weight PE and iPP, as well as of the ethylene-propylene-rubber (EPR) present in specific iPP grades.

Due to the relative ambiguity of the fractions eluting between 35 °C and 103 °C, it is important to couple these results with the information from CFC, i.e. accounting also for molecular weight dependences in the crystallization based fractionation from solution [57]. The CFC counterplot of REC3 is shown as an example for the complex chemical composition of iPP based recyclated in Fig. 11.

To further investigate the different fraction, iPP, HDPE, LDPE/LLDPE and EPR fraction the short chain branches per 1000 total carbon atoms (SCB/1000 TC) content along the molecular weight of the CFC fraction at 35 °C (A), 75 °C (B), 95 °C (C) and at 121 °C (D) were investigated.

Fig. 12A, describing the GPC-IR of the fraction eluting at 35 °C, shows probably the highest complexity as it can be expected since contributions of low molecular weight PE and iPP, as well as EPR rubber, can be expected. The first peak, with logM lower than ca. 3.2, can be attributed to low molecular weight iPP with minor contributions of low molecular weight PE, since SCB/1000 TC is in the order of 250. The second peak, at logM larger than 4, can therefore attributed to the EPR phase, with a higher content of ethylene in the ethylene-propylene copolymer in the range having SCB/1000 TC values between 150 and 230, corresponding to ethylene contents between 55 and 30 wt%.

The fraction eluting at 75 °C shows the very different behaviour of REC1-3 compared to the one of REC4. For the first set of materials, a SCB/1000 TC of ca. 30–50 implies that contributions from EPR rubber of other low molecular weight iPP fractions can be excluded. The very sharp and narrow elution peak at ~78 °C in the TREF profiles of Fig. 10 is typical for samples with a narrow ethylene sequence length distribution as it is present in LDPE [58] or LLDPE materials obtained from metallocene catalysts with a comonomer content between 3 and 4 mol% heptane or octene [59]. Due to the overwhelming market share of LDPE compared to LLDPE from metallocene catalysts, and to the source of the feedstock used to produce these materials, it can be concluded that this fraction is represented in vast majority by LDPE. However, in the case of REC1, the SCB/1000Tc increases at lower molecular weight, which is a typical observation if also non negligible amounts of low molar mass iPP are present. On the contrary, the higher SCB/1000 TC between 200 and 100 for REC4 indicates the presence of a higher amount of SCB, which can be explained by either by the presence of significant fraction of ethylene-propylene copolymers or ethylene-α-olefins. As

Table 4
Additional details on the microstructure of the materials studied, from fractionation studies.

	Instr.	Unit	REC1	REC2	REC3	REC4
iPP	CFC	wt%	69.3	41.9	45.3	78.2
HDPE (/EP)		wt%	11.7	24.2	23.2	6.0
LDPE (/EP/LLDPE)		wt%	12.9	29.7	27.1	6.8
SF (iPP/PE/EPR)		wt%	6.1	4.1	4.4	9.0
iPP	TREF	wt%	61.9	42.5	45.2	n.m.
HDPE (/EP)	TREF	wt%	12.9	23.9	18.9	n.m.
LDPE (/EP/LLDPE)	TREF	wt%	16.4	25.6	27.7	n.m.
SF (iPP/PE/EPR)	TREF	wit%	8.8	8.0	8.2	n.m.

ethylene-α-butene copolymers with a SCB/1000 TC content of 100 SCB/1000 TC would be elastomers, which would crystallise only at temperature below 20 °C in TCB, the high SCB/1000 TC content can only explained that the 75 °C fraction for Rec4 contains a significant amount of semicrystalline EP copolymers, which also would elute in the temperature fraction [60].

For the 95 °C fraction in Fig. 12C it can observed that the low molar mass peak for REC4 is at lower logM values, which can be explained because for REC4 the low molar mass tail is mainly composed of iPP, whereas this is not the case for REC1-3, where at the peak maxima at around logM of 4 a SCB/1000 TC level below 100 is observed, rather indicating low molar mass PE fractions.

For the CFC fraction eluting above 103 °C, it can be concluded from the plot in Fig. 12D for the GPC-IR of the 121 °C fraction that exclusively iPP is eluting, since the SCB/1000 TC shows a value of ~330.

It is worth to mention that recently another approach based on the CFC technique was published by Gora et al. [26], using the molecular weight of the iPP fraction eluting above 103 °C to back calculate the amount of iPP that would elute in elution temperatures below 103 °C. The main difference in the iPP content between the simple approach using just the CFC volume ratio and the approach discussed by Gora et al. is the application of the detector response correction, leading to slightly higher iPP content. This effect is mostly dominant in the range of 40–60 wt% content of iPP, as it is the case for REC 1–3.

This approach allows one to overcome the issues of comparing the PE/iPP content from NMR and DSC analysis to the ones obtained from CFC because of the contemporary presence of low molecular weight iPP in the fractions eluting at lower temperatures. For this reason, only these results are reported in Table 3, to compare to the other techniques. The full characterization from the fractionation experiments is instead reported in Table 4.

A good example of the implications from the presence of LDPE is given by rheology. The evaluation of the non-linear complexity of the materials is inferred from the LAOS-Non-Linear Factor (LAOS-NLF) parameter [61]. The analysed materials show a non-linear rheological behaviour stronger than the one expected for virgin linear material like LLDPE and HDPE. In this latter cases, LAOS-NLF of ca. 1.5 are measured, whereas values above 3 are obtained for virgin LDPE. The findings for the branching composition of REC1 and REC3, with LAOS-NLF values of ca. 2.3, are in general agreement with the presence of LDPE detected by CFC, DSC, NMR. However, we did not observe a large difference between REC1 and REC3, as it would have been expected only from the analytical results shown above. Thus it can be inferred that the non-linear behaviour is not only arising from the presence of branched chains alone, but also from the multiphase, complex composition of the

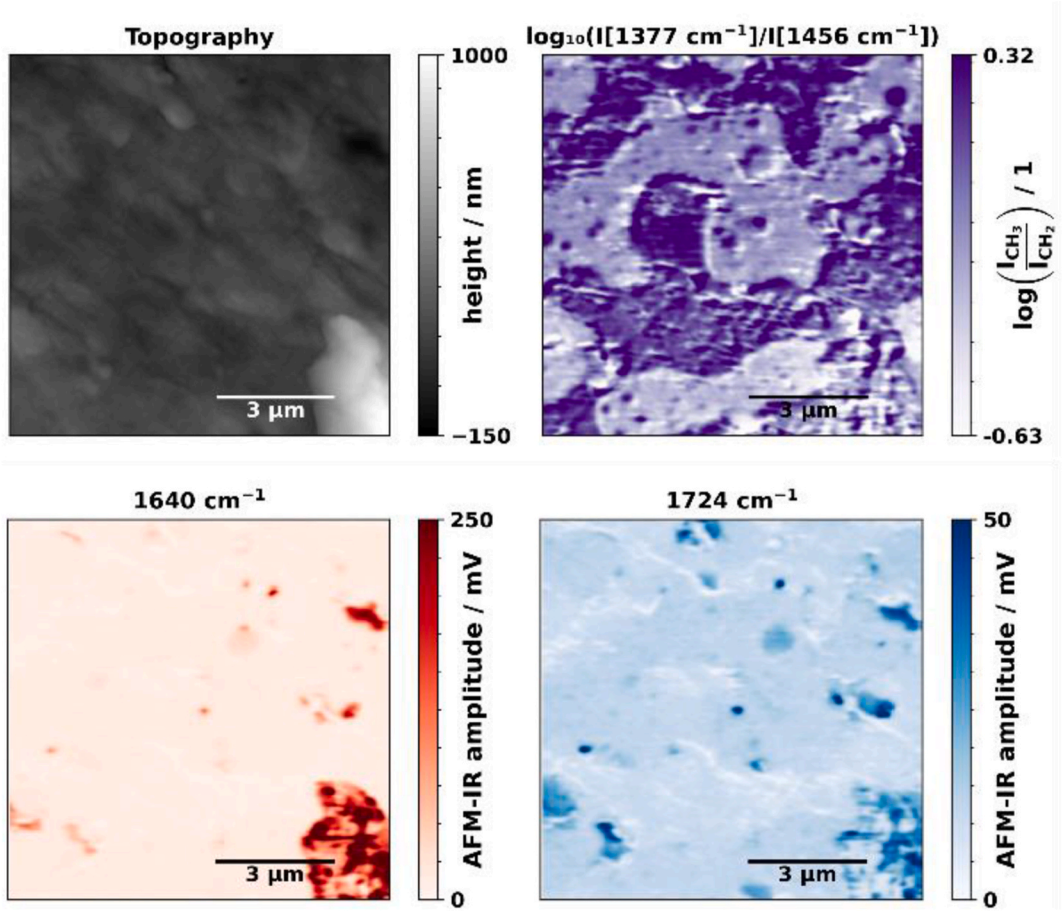

Fig. 13. AFM-IR image of REC3, clearly identifying the phase separated PE and iPP as well as some contaminations. Reproduced from Ref. [24] with permission from the Royal Society of Chemistry.

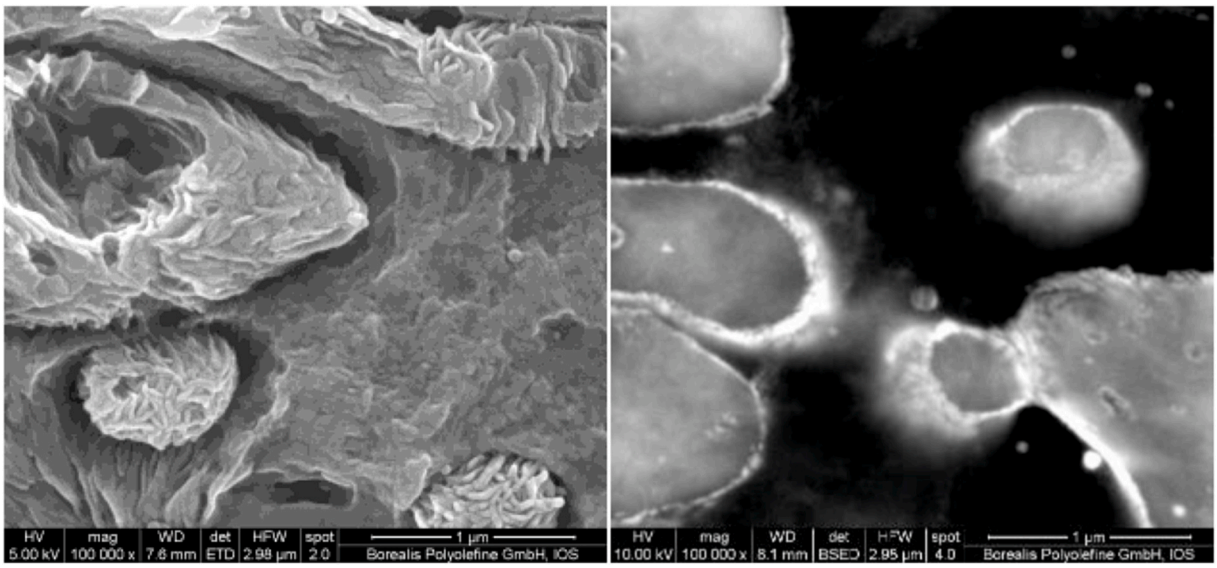

Fig. 14. On the left, morphology of the REC1 material in SEM after permanganic etching showing lamellae and PE domains with holes, indicating amorphous material inside. On the right, morphology of REC1 after RuO_4 staining, showing different components and in particular the EPR rubber as the bright areas.

materials.

Microscopies are able to provide additional information, in particular adding spatial resolution to the analytical techniques described above. Additionally, the presence of both PE and iPP has implications on the morphology developed and thus on final properties of the material. These two polymers are immiscible and therefore give rise to a phase separated structure. In a previous work, we used AFM-IR to image the PE and iPP phases, being able to unequivocally assign the identity of each phase through the ratio of the signals registered at the frequencies of 1377 cm^{-1} and 1456 cm^{-1}, see Fig. 13. Incidentally, this technique is also useful to image polymeric contaminations, and spectroscopically assign its nature, with far higher resolution of CT as shown in Fig. 13.

As shown before, SEM instead provides useful information about the inorganic contaminations however it also visualizes the morphology in great detail. One strategy for the analysis of the morphology of such materials is the introduction of topography into the samples, thus causing SEM contrast, and therefore adding the spatial information on the PE and iPP phases in addition to the analytical evaluations above. This can be achieved by selective removal of one phase. Here, oxidative degradation of the material with potassium permanganate ($KMnO_4$) under strongly acidic conditions was used. The fact that $KMnO_4$ reacts faster with the amorphous fraction of iPP and PE than with the crystalline fraction results in elevations corresponding to the crystalline fractions and dents where amorphous material was present. Therefore Fig. 14 shows lamellae visible after etching, and additionally also clearly shows dents where the EPR rubber was located, i.e. encapsulating the PE phase. The detailed knowledge of the morphology of elastomeric modifiers added to iPP/PE material is important for understanding the mechanical or optical properties of the final product.

In order to obtain clearer images and consequently further insight on the location of the EPR rubber, staining with RuO_4 was performed. In the case of polyolefins, RuO_4 reacts preferably with the amorphous phase inside of EPR particles. In this way the RuO_4 enriched amorphous phase displays increased elemental contrast compared to the crystalline phases and the three components (iPP/PE/rubber) are more clearly visible in Fig. 14. In particular the very bright areas in this figure refer to the EPR phase. This elemental contrast information can be visualized via different detectors, such as backscattered electrons (BSE) or scanning transmission electron microscopy (STEM) detector.

4. Conclusions

In this work, the combination of many different experimental techniques were used to extensively characterize recycled polyolefins. The choice of the materials REC1-3 used, and their thorough comparison with all the techniques discussed, allowed us to provide a glimpse of the variation that can be expected lot by lot in the case of using post-consumer recyclates. The addition of one random lot of REC4 also gave the opportunity to explore a comparison between different materials.

Inorganic contaminations were characterized by TGA as often found in the literature, however also by XRF, to obtain information about the presence of chalk and carbon black, which are extensively used additives to polyolefin commercial grades, as well as information about talc, TiO2, and various elements. This level of detail is required for a good understanding of the effect of inorganic contaminations on properties. CT and SEM allow one to add spatial resolution to this information, identifying size and shape of various contaminants. CT provides a statistically sound characterization, by measuring several pellets at once. SEM instead provided high resolution images, albeit on smaller areas. We also for the first time introduced an unconventional use of CT to quantify polymeric contaminations, based on their segmentation due to the different densities. FTIR spectroscopy in addition provided an ideal, spectroscopic identification of the contaminations albeit again on a smaller sample size. To cope with this, three FTIR spectroscopy measurements were repeated on three different plaques to discuss contaminations' content.

Finally, the complex microstructure arising from the fact that recycled materials are in fact a blend of several, very different virgin grades was investigated through NMR, DSC, TREF and CFC. It is worth mentioning that all these analysis were performed with methods optimized to study recycled materials and published elsewhere [26,27,37]. The results from the various techniques agree in general, although one must be careful to trust the results of only one technique alone. For example, NMR provides possibly the highest accuracy, at the price of a complex experimental technique and in particular being constrained by a relatively high limit of quantification for LDPE, set at ~20 wt%. On the other opposite, DSC is a simple technique that can be used also in quality control laboratories and the results, as shown in Table 2, agree fairly well with the ones from NMR. Finally, CFC is a very powerful technique which provides additional details on the various fractions, although if taken alone one should be very careful about the possible coelution of e.g. HDPE and ethylene-propylene copolymers or LDPE and LLDPE. Using

the results from CFC together with the more general characterization from CFC and DSC gives the clearest picture of the sample microstructure. In addition to these analytical techniques, AFM-IR and SEM, in the latter case with optimized etching or staining of the sample, also adds the spatial information, in order to visualize with very high resolution the details of the morphology developed by these complex materials.

CRediT authorship contribution statement

Davide Tranchida: Writing – review & editing, Writing – original draft, Project administration, Investigation, Formal analysis, Data curation, Conceptualization. **Dietmar Salaberger:** Writing – original draft, Investigation, Formal analysis, Data curation. **Lada Vukusic:** Writing – original draft, Formal analysis, Data curation. **Gerhard Hubner:** Writing – original draft, Investigation, Formal analysis, Data curation. **Mithun Goswami:** Writing – original draft, Formal analysis, Data curation. **Andreas Albrecht:** Writing – original draft, Formal analysis, Data curation. **Susana Filipe:** Writing – original draft, Project administration, Conceptualization.

Declaration of competing interest

The authors declare that they have no known competing financial interests or personal relationships that could have appeared to influence the work reported in this paper.

Appendix A. Supplementary data

Supplementary data to this article can be found online at https://doi.org/10.1016/j.polymer.2024.127970.

Data availability

The data that has been used is confidential.

References

[1] E. De Tandt, C. Demuytere, E. Van Asbroeck, H. Moerman, N. Mys, G. Vyncke, L. Delva, A. Vermeulen, P. Ragaert, S. De Meester, K. Ragaert, Waste Manag. 119 (2021) 315–329.
[2] H. Oksana, C. Andrea, D.-L. Daniel, F. Andres, "Applications and future of recycling and recycling plastics" in Recent Developments in Plastic Recycling, p 345-372 Springer.
[3] K.S. Prado, M. Strangl, S.R. Pereira, A.R. Tiboni, E. Ortner, M.A.S. Spinace, A. Buettner, Waste Manag. 115 (2020) 36–46.
[4] A. Bunjes, J.-H. Arndt, G. Geertz, B. Barton, Polymer 249 (2022) 124823.
[5] K.S. Boparai, R. Singh, F. Fabbrocino, F. Fraternali, Composites, Part B 106 (2016) 42–47.
[6] S. Chong, G.-T. Pan, M. Khalid, T.C.-K. Yang, S.-T. Hung, C.-M. Huang, J. Polym. Environ. 25 (2017) 136–145.
[7] I. Michalska-Pozoga, T. Rydzkowski, P. Mazur, O. Sadowska, V.K. Thakur, Vacuum 146 (2017) 641–648.
[8] N. Fantuzzi, A. Vidwans, A. Dib, P. Trovalusci, J. Agnelli, A. Pierattini, Structures 57 (2023) 104966.
[9] P.O. Tawiah, P.Y. Andoh, A. Agyei-Agyemang, F. Nyarko, J. Intern, Of Sci. And Techn., vol. 5, 2016, p. 259.
[10] A.-H. Chiou, C.-H. Lin, Heliyon 9 (2023) e19403.
[11] Y.V. Vazquez, S.E. Barbosa, Waste Manag. 53 (2016) 196–203.
[12] M.R. Monteiro, D.G.G. Moreira, M.A. Chinelatto, P.A.P. Nascente, N.G. Alcantara, J. Polym. Environ. 15 (2007) 195–199.
[13] B. Hu, S. Serranti, N. Fraunholcz, F. Di Maio, G. Bonifazi, Waste Manag. 33 (2013) 574–584.
[14] I. Jonkkari, V. Poliakova, V. Myllsri, R. Anderson, M. Andersson, J. Vuorinen, J. Appl. Polym. Sci. 137 (2020) 49101.
[15] A.P. Adam, J.V.R.V. Gonçalves, L.C. Robinson, L.C.d. Rosa, E.L. Schneider, Mater. Res. 20 (2) (2017) 202.
[16] S. Filipe, P.M. Mourao, N. Couto, D. Tranchida, Polymers 15 (2023) 4529.
[17] M. Alzerreca, M. Paris, O. Boyron, D. Orditz, G. Louarn, O. Correc, Polym. Test. 46 (2015) 1–8.
[18] S. Bertin, J.-J. Robin, Eur. Polym. J. 38 (2002) 2255–2264.
[19] J.A. Rodriguez-Liebana, M.A. Martin-Lara, F.J. Navas-Martos, A. Penas-Sanjuan, V. Godoy, S. Arjandas, M. Calero, Journ. Of environm, Chemical Eng 10 (2022) 108332.
[20] I.S. Sani, N.R. Demarquette, E. David, Polym. Eng. Sci. 63 (2023) 3254–3267.
[21] M. Gall, P.J. Freudenthaler, J. Fischer, R.W. Lang, Polymers 13 (2021) 1574.
[22] L. Cozzarini, L. Marsich, A. Ferluga, Polym. Eng. Sci. 63 (2023) 1126–1132.
[23] S.A. Stoian, A.R. Gabor, A.-M. Albu, C.A. Nicolae, V. Raditoiu, D.M. Panaitescu, Journ. Of thermal, Anal. And Calorim 138 (2019) 2469–2480.
[24] R. Juan, B. Paredes, R.A. Garcia-Munoz, C. Dominguez, Polym. Test. 100 (2021) 107273.
[25] M. Hashemnejad, A. Doshi, Polym. Test. 139 (2024) 108577.
[26] J.C.M. Suarez, E.B. Mano, Polym. Degrad. Stabil. 72 (2021) 217–221.
[27] A.G. Pedroso, D.S. Rosa, Carbohydrate Polym. 59 (2005) 1–9.
[28] A.C.V.D. Dos Santos, D. Tranchida, B. Lendl, G. Ramer, Analyst 147 (2022) 3741–3747.
[29] I.I. Cuesta, J.M. Alegre, C. Rodriguez, Journ. Of appl, Polym. Sci. 133 (2015) 42911.
[30] M. Gora, D. Tranchida, A. Albrecht, A.J. Müller, D. Cavallo, Polym. Test. 131 (2024) 108351.
[31] A. Scoppio, D. Cavallo, A.J. Müller, D. Tranchida, Polym. Test. 113 (2022) 107656.
[32] A. Scoppio, S. Coba-Daza, D. Cavallo, D. Tranchida, A.J. Müller, Polymer 302 (2024) 127045.
[33] S. Coba-Daza, A. Albrecht, D. Cavallo, D. Tranchida, A.J. Müller, Journ. Of Thermal Anal. And Calorim, 2024, pp. 1–13.
[34] M. Gora, S. Coba-Daza, E. Carmeli, D. Tranchida, A. Albrecht, A.J. Müller, Polymer 282 (2023) 126180.
[35] M. Gora, D. Tranchida, A. Albrecht, A.J. Müller, D. Cavallo, J. Polym. Sci. 60 (2022) 3366–3378.
[36] G. Singh, A. Kothari, V. Gupta, Polym. Test. 28 (5) (2009) 475.
[37] Z. Zhou, R. Kuemmerle, X. Qiu, D. Redwine, R. Cong, A. Taha, D. Baugh, B. Winniford, J. Magn. Reson. 187 (2007) 225.
[38] V. Busico, P. Carbonniere, R. Cipullo, R. Pellecchia, J. Severn, G. Talarico, Macromol. Rapid Commun. 28 (2007) 1128.
[39] A. Ortin, B. Monrabal, J. Sancho-Tello, Macromol. Symp. 257 (2007) 13–28.
[40] ISO 3451-1:2019 - Plastics — Determination of Ash.
[41] E. Karaagac, M.P. Jones, T. Koch, V.-M. Archodoulaki, Polymers 13 (2021) 2618.
[42] T. Kinoshita, T. Yamamoto, C. Luo, K. Ide, K. Aoki, Y. Uetsuji, Compos. B Eng. 266 (2023) 110971.
[43] J. Maurer, D. Salaberger, M. Jerabek, B. Fröhler, J. Kastner, Z. Major, Polym. Test. 130 (2024) 108313.
[44] V. Morgado, L. Gomes, R.J.N. Bettencourt da Silva, C. Palma, Talanta 234 (2021) 122624.
[45] V. Busico, P. Carbonniere, R. Cipullo, R. Pellecchia, J. Severn, G. Talarico, Macromol. Rapid Commun. (2007) 1128.
[46] V. Busico, R. Cipullo, A.L. Segre, Macromol. Chem. Phys. 203 (2002) 1403.
[47] Z. Zhou, R. Kuemmerle, X. Qiu, D. Redwine, R. Cong, A. Taha, D. Baugh, B. Winniford, J. Magn. Reson. 187 (2007) 225.
[48] S.K. Sahoo, T. Zhang, D.V. Reddy, P.L. Rinaldi, Macromolecules 36 (2003) 4017.
[49] W.-J. Wang, S. Zhu, Macromolecules 33 (2000) 1157.
[50] J. Randall, Macromol. Sci., Rev. Macromol. Chem. Phys. 201 (1989).
[51] G. Hubner et al, submitted for publication.
[52] W. Liu, D.G. Ray, P.L. Rinaldi, Macromolecules 32 (1999) 3817.
[53] D.C. Bugada, A. Rudin, Eur. Polym. J. 23 (1987) 809.
[54] F.A. Bovey, F.C. Schilling, F.L. McCrackin, H.L. Wagner, Macromolecules 9 (1976) 76.
[55] J.C. Randall, C.J. Ruff, M. Kelchtermans, Recl. Trav. Chim. Pays-Bas 110 (12) (1991) 543.
[56] M.J. Caballero, I. Suarez, B. Coto, R. Van Grieken, B. Monrabal, Macromol. Symp. 257 (2007) 122.
[57] L. Wild, G. Glöckner Temperature Rising Elution Fractionation Separation Techniques Thermodynamics Liquid Crystal Polymers, Springer Berlin Heidelberg, Berlin, Heidelberg, 1991, pp. 1–47.
[58] P.L. Joskowicz, A. Muiioz, J. Barrera, A.J. Müller, Macromol. Chem. Phys. 196 (1995) 385.
[59] E. Cossoul, L. Baverel, E. Martigny, T. Macko, C. Boisson, O. Boyron, Macromol. Symp. 330 (2013) 42–52.
[60] B. Monrabal, Adv. Polym. Sci. 257 (2013) 203–252.
[61] S. Filipe, K. Klimke, A.T. Tran, J. Reussner, AIP Conf. Proc. 1375 (2011) 114.